CrossMark

Simultaneous enhancement of room temperature multiferroic properties of BiFeO$_3$ by Nd doping at Bi site and Co doping at Fe site

I. B. Shameem Banu[1] · S. Divya Lakshmi[1]

Abstract Room temperature ferroelectric and magnetic properties of undoped BiFeO$_3$ and (Nd, Co) codoped BiFeO$_3$ are reported. The sol–gel synthesized Bi$_{1-x}$Nd$_x$Fe$_{0.98}$Co$_{0.02}$O$_3$ (x = 0.01, 0.02, 0.03, 0.04, 0.05 and 0.06) ceramics were analysed by XRD pattern, Raman spectrum, X-ray photoelectron spectrum (XPS), ferroelectric loop and magnetic hysteresis loop. The evolution of the changes in the ferroelectric and magnetic properties with gradual tiny increase in the dopant concentration was investigated. XRD patterns and Raman spectra confirm the typical rhombohedral structure for all the samples. The oxidation states of Fe and the existence of oxygen vacancies studied through XPS reveal that enhanced ferroelectric properties of the doped samples are due to the presence of low Fe^{2+} ions and reduction of oxygen vacancies. The remnant polarisation and maximum polarisation values of Nd 1–5% doped samples are remarkably enhanced compared to BFO. The highest Nd doping 6% showed reduced ferroelectric parameters due to the internal strain caused by the high doping, which was illustrated by its Raman spectrum. Well saturated magnetic hysteresis loops are obtained due to the doping of Nd and Co with significant magnetic parameters. A notable simultaneous improvement in both magnetic and ferroelectric properties has been illustrated for 1–5% of Nd doping.

1 Introduction

Multiferroic materials possess magnetic and ferroelectric order simultaneously to exhibit coupling between these two orders and this coupling leads to several applications because of their ability for electric control of magnetism and vice versa [1–5]. Bismuth ferrite, BiFeO$_3$ (BFO), is the most widely explored multiferroic, since it exhibits multiferroicity at room temperature. At room temperature, BFO has rhombohedrally distorted pervoskite (space group R3c) structure. Its ferroelectric curie temperature T$_C$ is 830 °C and it exhibits antiferromagnetism up to the Neel temperature of T$_N$ = 375 °C [6]. It shows a G-type canted antiferromagnetic order below T$_N$ [7, 8] due to the spin spiral structure of period 62 nm. Its room temperature coupling between ferroelectricity and magnetism is of key significance for several applications. However, BFO has a little disadvantage of being impure, leaky in current and low in magnetism. Preparation of BFO free of impure phases is a challenge. The impurity phases are mainly due to the existence of Bi and Fe in BFO and volatile nature of BFO. The ferroelectric hysteresis of BFO may not saturate due to its high leakage current density. The reason for weak magnetism in BFO may be attributed to the incommensurate spin cycloid structure of BFO which cancel the spins to a large extent resulting in canted antiferromagnetism. If the spin spiral structure is disrupted to obtain a net magnetic moment, BFO can be used suitably in enormous applications.

These minor disadvantages faced by BFO can be suppressed by doping it with suitable element in the BFO lattice. Several researches about doping have been reported, such as Bi-site substitution with rare earth or alkaline earth elements and Fe-site substitution with transition metals. Recently, numerous works were reported,

✉ I. B. Shameem Banu
  shameembanu@bsauniv.ac.in

[1] Department of Physics, B. S. Abdur Rahman University, Chennai, Tamil Nadu, India

concerning simultaneous A and B site co-doping with two different elements to enhance its multiferroic properties. Mainly, the substitution at Bi site is expected to reduce the volatility of Bi to enhance ferroelectric character while Fe site doping can break the spin cycloid structure to improve the magnetic characteristics of BFO.

For instance, Quan et al. have done a work on Nd and Ca co-substituted BFO, which reveals an enhancement in magnetism [9]. Hernandez et al. reported a work on Nd and Sc co-doped BFO, in which ferromagnetic behaviour has been improved at room temperature [10]. Raghavan et al. studied Nd and Zn co-doped BFO thin film using chemical solution deposition method, which showed enhanced magnetization compared to BFO thin film [11]. Raghavan et al. investigated Nd and Cu co-doped BFO thin film synthesized using chemical solution deposition method, in which significant improvement in the electric and ferroelectric properties was observed [12]. Khomchenko et al. reported about (Nd, Mn) doped BFO and revealed structure phase transformation from polar state to non-polar one with increasing Nd concentration, with enhanced magnetization [13]. Hernandez et al. [14] reported the ferromagnetic behaviour of Nd and Co codoped BFO and Godara et al. [15] showed well developed magnetic hysteresis loop for Nd and Co/Cr doped BFO for Nd 5 and 10% at Bi site and Co (Cr) 5% at Fe site. So far, ferroelectric study and magnetoelectric coupling effect on Nd, Co codoped BFO have not been investigated and also the effect of low concentration of Nd and Co on the magnetic and ferroelectric properties have not been explored. A thorough investigation of low level doping to BFO will bring out the evolution of the changes in the structure and hence the resulting variation in the multiferroic properties. Such a study on the gradual addition of the dopant in BFO will reveal its influence on tuning the ferroelectric, magnetic properties and magnetoelectric coupling. Moreover, as far as we know, there are only some reports on magnetic ion Co codoped to BFO with rare earth ion at Bi site. They are (La, Co) co-doped [16] and (Eu, Co) co-doped [17] in which Co is at a high (5%) doping concentration at Fe site. Among the several reports on dual doping of elements at Bi site and Fe site, studies on the Nd doping with other elements is scanty. Hence, Nd doped with Co demands a systematic investigation of both ferroelectric and magnetic properties. So in this work, we report the magnetic and ferroelectric properties of $Bi_{(1-x)}Nd_{(x)}Fe_{0.98}Co_{0.02}O_3$ (x = 1–6%) samples and the effect of the multiferroic properties on the tiny addition of Nd at Bi site (1–6%) with Co dopant fixed at low level of 2% at Fe site in the BFO lattice is investigated. This work brings out the evolution of the ferroelectric and magnetic features of the low level doped

BFO and provides the reasons for variation of these properties in detail.

1.1 Experimental details

$BiFeO_3$ (BFO) and $Bi_{1-x}Nd_xFe_{0.98}Co_{0.02}O_3$ (x = 0.01, 0.02, 0.03, 0.04, 0.05 and 0.06) ceramics were prepared using sol–gel method. In further discussion, $Bi_{1-x}Nd_xFe_{0.98}Co_{0.02}O_3$ will be denoted respectively as BNFCO1, BNFCO2, BNFCO3, BNFCO4, BNFCO5 and BNFCO6 corresponding to 1–6% doping of Nd at Bi site of BFO. Analytical grade Bismuth(III) Nitrate pentahydrate (assay 98%, Alfa Aesar), Iron(III) Nitrate Nonahydrate (assay 98%, Alfa Aesar), Neodymium(III) Nitrate Hexahydrate (assay 99.9%, Alfa Aesar), Cobalt(II) nitrate hexahydrate (assay 99.999%, Alfa Aesar), Citric acid anhydrous (assay 99.5% Merck) and nitric acid (assay 70% Merck) were used as starting materials without any further purification, as all the chemicals were of analytical grade. The starting material weighed according to the stoichiometric ratio were dissolved in the distilled water and the prepared solution was stirred well at 400 rpm for some time to obtain homogenization. Then the mixture was heated on hot plate at 80 °C and stirred continuously till it became dark viscous resin. When the gelation happened, the temperature was increased slightly until auto combustion of dried resin took place with the evolution of large amount of gases. The resulting powder was then ground into fine powder using agate mortar and pestle. The fine powder was sintered at 800 °C for 4 h in a high temperature furnace. For electrical measurements, powders were pelletized using a hydraulic pellet press by applying a pressure of 6 tons and annealed at 700 °C for 4 h in a high temperature furnace. The silver paste was coated on both the side of the pellet to get conductivity.

The phase of the samples were identified using X'Pert Pro X-ray Diffractometer (PANalytical) with Cu K_{α} radiation for the Bragg angle range of 10°–70° at the scanning rate of 0.04 min^{-1}. Raman spectrum was recorded using Laser confocal Microscope with spectrometer (inVia Raman, Renishaw, UK) to analyse the structural evolution of the doped samples with increase in dopant concentration. Composition of the prepared samples, oxidation states of Fe and the presence oxygen vacancies in the samples were analysed through XPS spectrum (K alpha model and make Thermo fisher scientific UK). The room temperature ferroelectric properties were measured using ferroelectric (P-E) loop tracer (Marine India Pvt. Ltd). The magnetization hysteresis (M-H) loop of the samples were measured at room temperature using vibrating sample magnetometer (EG & G PARC VSM 155).

2 Results and discussion

The XRD patterns of all the undoped and doped samples are displayed in Fig. 1a. These patterns show that all the samples have the polycrystalline rhombohedral structure of space group R3c which is in confirmation with the JCPDS card no (86–1518). The (012) peak at around 22°, the splitting of the (104) and (110) peaks around 32° and the splitting of the (006) and (202) peaks around 40° confirm the rhombohedral structure of the samples. Small traces of impurity phases $Bi_2Fe_4O_9$ (Mullite) are observed for undoped BFO and the presence of these impurity phases decreases when Nd and Co are doped to BFO. With increase in Nd doping concentration, these impurity phases disappear completely for 4 and 5% Nd. In the case of 6% Nd doping, the small traces of impurity phases reappear and this is may be due the strain induced by the higher Nd concentration. The impurity phases appear in the XRD pattern due to the non-volatile nature of Bi^{3+} ions. So, the absence of impurity peak for the doped samples indicates that the Bi–O bond is stabilised due to Nd being doped at Bi site. As the bond dissociation energy of Nd–O (703 eV) is more than that of Bi–O bond (337.2 eV), the volatility of Bi is reduced and the oxygen vacancies are also expected to be reduced. The disappearance of impurity phases due to doping of ions may result in improved ferroelectric properties of doped BFO compared to undoped BFO. It is clear from the sharp XRD peaks that doping has led to good crystallinity of the ceramics. The variation in the intensity and the peak position confirm the incorporation of Nd and Co in the BFO lattice. The enlarged XRD patterns for the (012) and (110) peaks are shown in Fig. 1b, c respectively. The diffraction peaks (012) and (110) shift towards the higher Bragg angle for all the doped samples relative to that of BFO, indicating the decrease in the lattice parameters due to the substitution of Nd at Bi site and Co at Fe site. As the radius of Nd^{3+} ion (1.109 Å) is less than that of Bi^{3+} (1.17 Å), the shift towards lower angle occurs with increase in the Nd doping level. The crystallite sizes calculated from the XRD data of (110) peak using the Debye Scherrer formula are 51, 48, 47, 45, 39 and 47 nm respectively for BNFCO1, BNFCO2, BNFCO3, BNFCO4, BNFCO5 and BNFCO6 samples.

The lattice parameters a and c and volume of the unit cell were calculated using UnitCellWin software using the XRD data and the obtained a and c were used to calculate the bond angles and rhombohedral unit cell using VESTA software. Table 1 summarises the lattice parameters, volume, bond lengths and the bond angle of the rhombohedral structure for the BFO, BNFCO1, BNFCO2, BNFCO3, BNFCO4, BNFCO5 and BNFCO6 samples. From this table, it is clear that Fe–O–Fe bond angle decreases when Nd and Co are doped to BFO lattice revealing the changes in the Fe–O–Fe bond angle which provides the evidence for the disruption in the spin cycloid structure due to Bi and Fe site substitution, leading to enhanced ferromagnetism. The lattice parameters are observed to decrease when doped, resulting in contraction of volume of the unit cell and this is in corroboration with the XRD peak shifts as discussed earlier. Bi–O and Fe–O bond lengths are found to
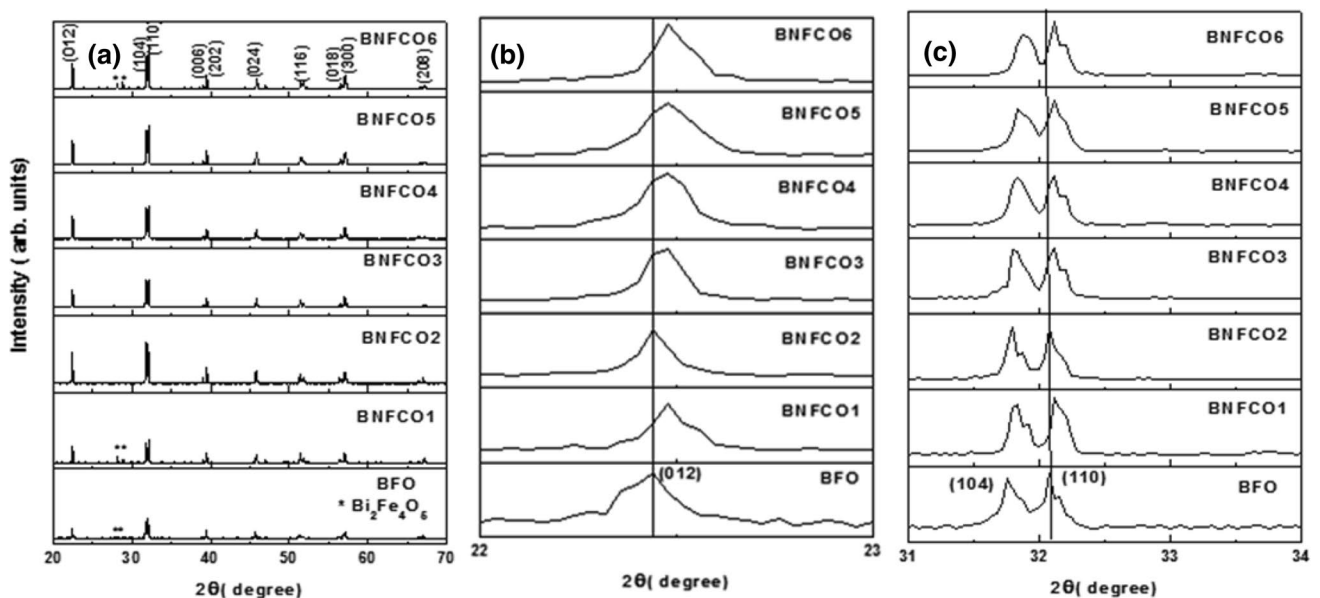

Fig. 1 XRD patterns of BFO, BNFCO1, BNFCO2, BNFCO3, BNFCO4, BNFCO5 and BNFCO6 and magnified XRD peaks of (012), (104) and (110)

Table 1 Lattice parameters (a–c), unit cell volume V, bond lengths Bi–O, Fe–O and bond angle Fe–O–Fe

Sample	a (=b) (Å)	c (Å)	V (Å³)	Bi–O (Å)	Fe–O (Å)	Fe–O–Fe (°)
BFO	5.5787	13.8688	373.797	2.4727	2.0855	154.3217
BNFCO1	5.5625	13.8204	370.3301	2.4654	2.0785	153.3567
BNFCO2	5.5725	13.8291	371.8978	2.4627	2.0770	153.3269
BNFCO3	5.5681	13.8139	370.9034	2.4677	2.0793	153.3188
BNFCO4	5.5673	13.8145	370.8062	2.4673	2.0791	153.3238
BNFCO5	5.5664	13.8018	370.3577	2.4668	2.0782	153.3042
BNFCO6	5.5646	13.8026	370.1308	2.4661	2.0778	153.3140
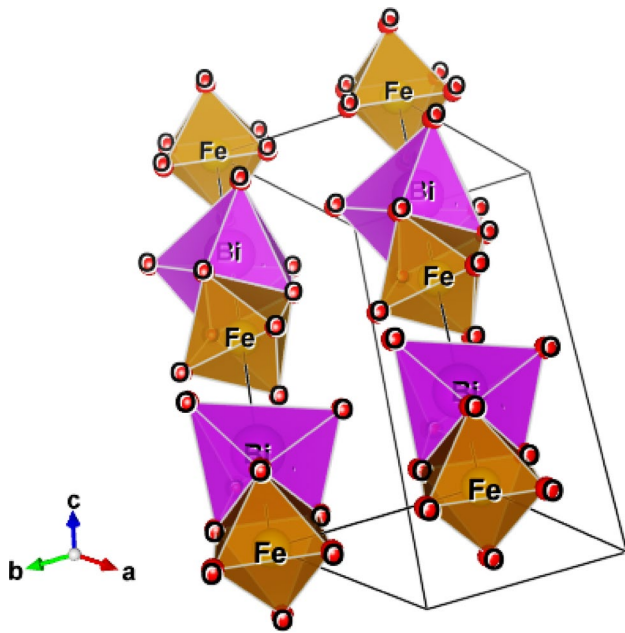
Fig. 2 The unit cell of rhombohedral BFO generated using VESTA software. The FeO_6 octhedra are titled along the c axis

decrease when doped. Figure 2 shows the unit cell of rhombohedral BFO generated using VESTA software, in which FeO_6 octahedra and tilting of octahedra along the c axis are exhibited.

Figure 3 shows the Raman spectra of all the samples at room temperature. The 13 Raman active modes of rhombohedral R3c structure can be summarised using the irreducible representation $\Gamma = 4A_1 + 9E$ [18]. All the modes are present for the undoped and doped samples. Figure 3 shows that the number of Raman modes remain unchanged with increase in the doping concentration of Nd, which clearly indicates that all the doped samples are in rhombohedral structure. However, relative change in the intensity and position is observed due to the effect of doping. In general, compared to BFO, the peak intensities of almost all the Raman modes exhibit an increase in intensity, when Nd and Co are doped. This confirms the incorporation of Nd and Co in the BFO lattice. Enhanced intensity is due to the

strong stretching and bending modes of Bi–O and O–Fe–O and FeO_6 octahedran [19]. Any shift in the positions of the Raman peaks or change in the intensity are the clear indication of the change in the bond length or change in the mass of the ions involved. So, the changes in intensity and peak position speculate that strain or lattice distortion is involved due to doping in the parent lattice. The low frequency A_1 and E (E_1 and E_2) modes are attributed to vibration modes of Bi–O and the high frequency E modes are related to the Fe–O vibration [20, 21]. The modes around 77 and 137 (E_1 and E_2) and 172 cm^{-1} (A_1) corresponds to the vibration of Bi–O bonds and are responsible for the ferroelectric nature of the bismuth ferrite [22]. So, changes in the ferroelectric properties are related to the changes in the peak intensity of these modes. In the case of BFO, the peak at lower frequencies <200 cm^{-1} is observed to be broadened whereas for the doped samples, the peaks are sharp upto 5%. However, for 6%, the peak broadening in the low frequency is visible and this is attributed to the internal strain induced as discussed in XRD details. The A_1 peak is strong in intensity for all the samples except for 6%. In the case of 6%, the peak intensity has reduced for all Raman modes and this may be due to the strain caused in the lattice due to higher doping concentration. So, in the case of 6% Nd, the ferroelectric parameters show low values compared to other doped samples which is discussed in the later section.

The X-ray photoelectron spectrum was recorded to know the oxidation states of Fe, the presence of oxygen vacancies and to confirm the composition of the samples. The XPS spectra for Nd 1, 3 and 4% were recorded for the range of 0–1200 eV and are presented in Fig. 4. These three were selected as sample for the varied Nd concentration in order to understand the ferroelectric and magnetic properties of the doped BFO. The binding energy peaks of Bi, Fe, O, Nd and Co are present in the spectra (Fig. 4a) confirming presence of the dopants Nd and Co and the main elements of BFO in the samples. The absence of impurity peaks indicate the high purity of the sample. The peak corresponding to C is present as it is used for calibration. The oxidation states of Fe were investigated through the XPS spectra. The binding energy of Fe $2P_{3/2}$ is expected to be at 709 eV for Fe^{2+} and 710 eV for Fe^{3+} [23]. To determine
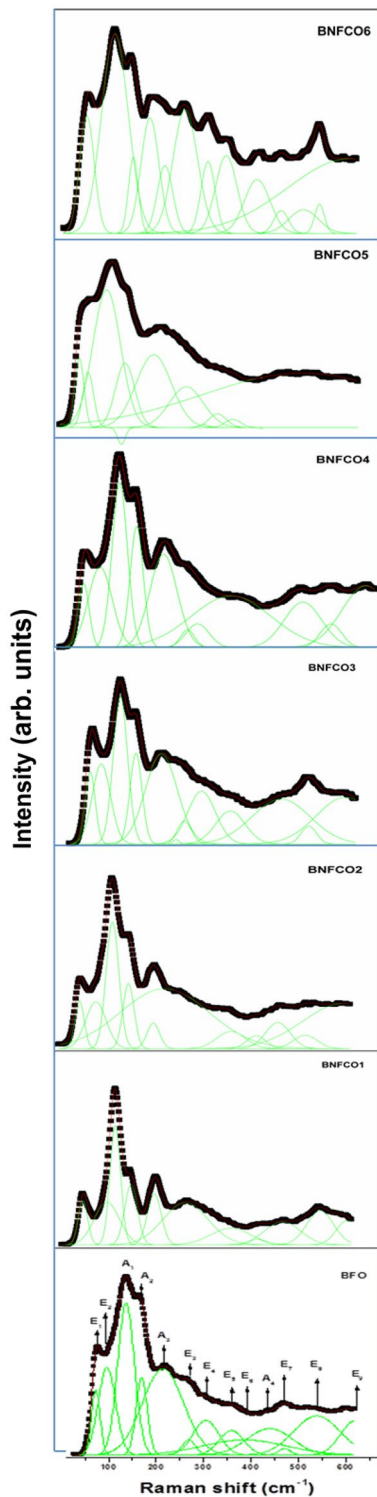
Fig. 3 Raman spectra of BFO, BNFCO1, BNFCO2, BNFCO3, BNFCO4, BNFCO5 and BNFCO6

the coexistence of Fe^{2+} and Fe^{3+}, the Fe $2P_{3/2}$ core level peaks were fitted to the Gaussian function and are shown in Fig. 4b. The calculated $Fe^{3+}:Fe^{2+}$ ratio is 1:0.49, 1:0.32 and

1:0.52 respectively for 1, 3 and 4% of Nd which shows that Fe^{3+} dominates over Fe^{2+} in the doped samples. Hence, this also suggests that Fe–O–Fe electron hopping is reduced for the (Nd, Co) doped samples and so the ferroelectric properties should enhance for the doped samples, which will be discussed in further sections.

In order to study the presence of the oxygen vacancies, the XPS peaks of oxygen were fitted and are shown in Fig. 4c. The peak located at 529 eV is attributed to the binding energy of intrinsic O^{2-} ion and this peak is visible in all the three samples. If there is O^{2-} vacancy, a peak at the binding energy 533.5 eV should be present. While this peak is present at 533.5 eV for 1%, for the higher Nd doping (Nd 3% and Nd 4%), this peak is absent indicating the absence of O^{2-} vacancy. However, the O^{2-} vacancy defects can not be ignored completely as the level of oxygen vacancy might be too low to be detected within the instrument limits. So, for higher Nd doping (3, 4%), O^{2-} vacancies are too low to be detected and this speculates that higher concentration of Nd reduces the oxygen vacancies.

Figure 5 presents the room temperature ferroelectric (P-E) loops of undoped and doped samples. The values of remnant polarization P_r and maximum polarization P_{rmax} are presented in Table 2. It is seen that undoped BFO exhibits an unsaturated P-E loop having rounded shape indicating the current leakage behaviour of BFO. Preparation of BFO, free of impurity phases is a challenge due to the volatility of Bi, which is in general a major reason for its leaky nature. The P_r value of undoped BFO is 0.838 μC/cm². However, when doped with Nd and Co, the shape of the P-E loops illustrate a remarkable improvement by exhibiting well developed P-E loops. With the increase in the Nd doping concentration, it is observed that the P_r value of 2–5% Nd enhances significantly. However, for 6%, the P_r value has decreased and also its P-E loop shape is distorted compared to the other doped samples and this difference has been illustrated from the Raman spectrum in the earlier section. Hence, this systematic study on ferroelectric properties of tiny dopant at BFO lattice speculates that the ferroelectric properties diminish when Nd level in the BFO lattice is increased beyond a certain limit. So, this sort of study paves way to the tuning of ferroelectric properties by appropriate dopant limit. From values of the crystallite sizes, it is clear that crystallite size decreases gradually with increase in Nd doping up to 5% while for 6%, it increases abruptly and so the diminished ferroelectric parameters of 6% may be associated with this increase.

When Nd 1% is doped to BFO, the PE loop is improved exhibiting an elongated loop compared to BFO. On further rise in the Nd doping, for Nd 2–5% samples, the shape of the loops improves remarkably and so it indicates clearly that the doping of Nd at Bi site decreases the volatility of Bi and hence reduces the presence of oxygen vacancies.
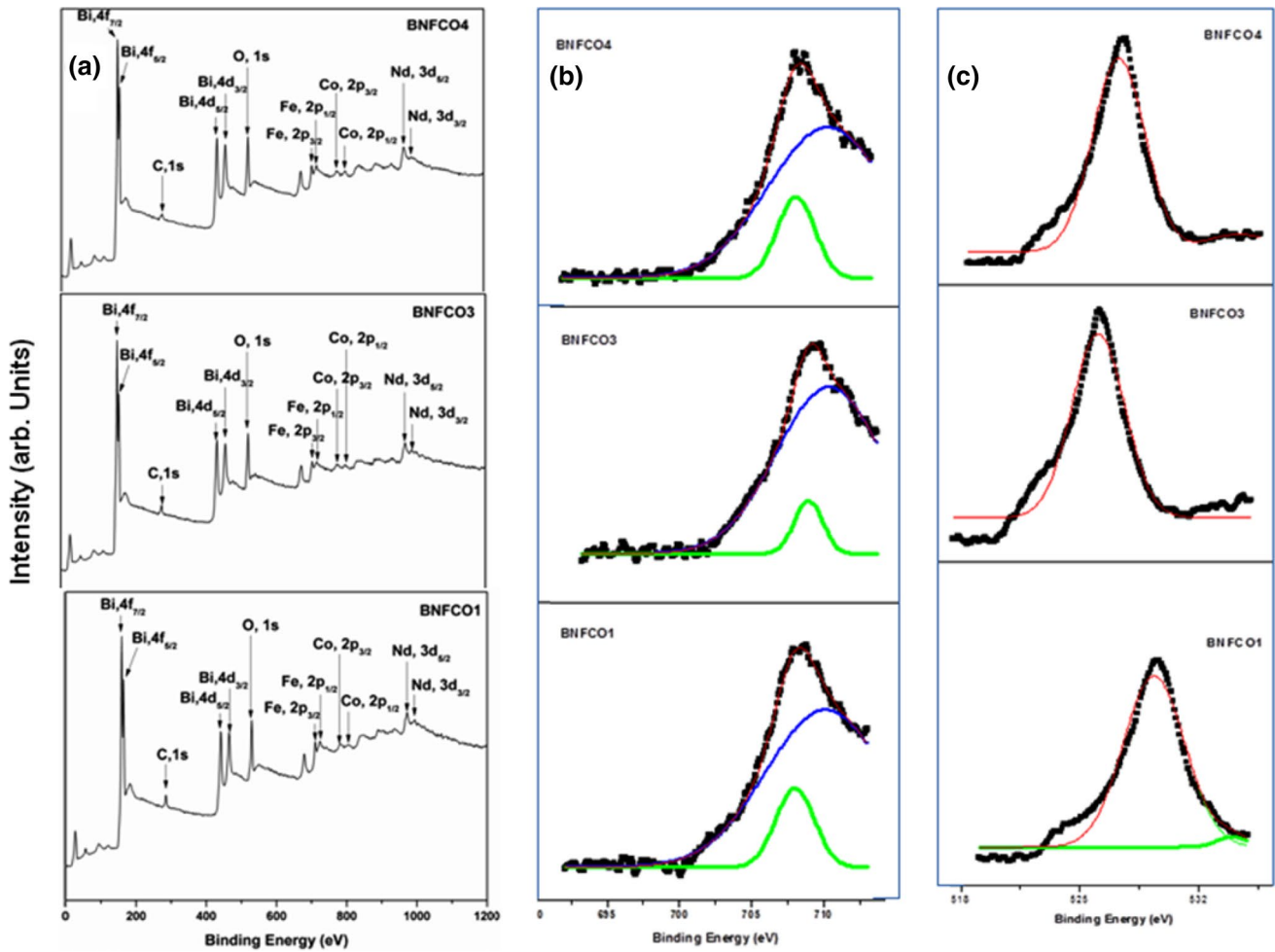
Fig. 4 XPS spectrum of BNFCO1, BNFCO3 and BNFCO4

The presence of oxygen vacancies and virtual hopping of electrons between Fe^{3+} and Fe^{2+} are the main reasons for the leakage current of the samples and for the deterioration of ferroelectric parameters. In our study, the XPS spectrum provides the evidence for the reduction of oxygen vacancies and reduction of Fe^{2+} ions compared to Fe^{3+} ions, with Nd doping increase and so the ferroelectric properties are significantly improved with Nd increase in the BFO lattice. The enhancement in the P-E loop with the dopant concentration is understood from the changes in the Raman peak intensity of these samples and it is explained as follows. The intensity of the peaks for Bi–O vibration which are related to the ferroelectric properties increases with Nd doping concentration increase. In particular, with increase in the dopant concentration, the intensity of the prominent Raman peak A_1 (Bi–O vibration) increases relative to that of BFO. The occurance of vibrant P-E loop of 2–5% are attributed to this increase in intensity of A_1 mode. For 6% Nd doped case, the intensity is reduced when compared to other 5 samples and this may be attributed to the high Nd level that causes stress in the lattice, leading to domain pinning effect and this effect may restrict the polarization. In summary, the P-E results speculate that doping Nd and Co enhances the ferroelectric properties of BFO and high concentration of Nd affects the ferroelectric property.

The magnetic hysteresis loops (M-H curve) measured at room temperature for the all the samples are shown in Fig. 6. The inset corresponds to the M-H curve of BFO sample. The ferromagnetic parameters such as saturation magnetisation M_s, retentivity M_r and coercivity H_c are presented in the Table 2. The M-H loops of all the doped samples are well saturated with the typical ferromagnetic M-H curve demonstrating the enhanced ferromagnetic properties of the Nd and Co doped samples as compared to that of BFO. The hysteresis loop for BFO shows a very weak ferromagnetism in contrast to typical antiferromagnetism as the crystallite size of the BFO is in the nano level (26 nm) and moreover, the periodic structure can be broken due to dimensional limitations resulting the collapse of spin cycloid structure which is considered to be major reason
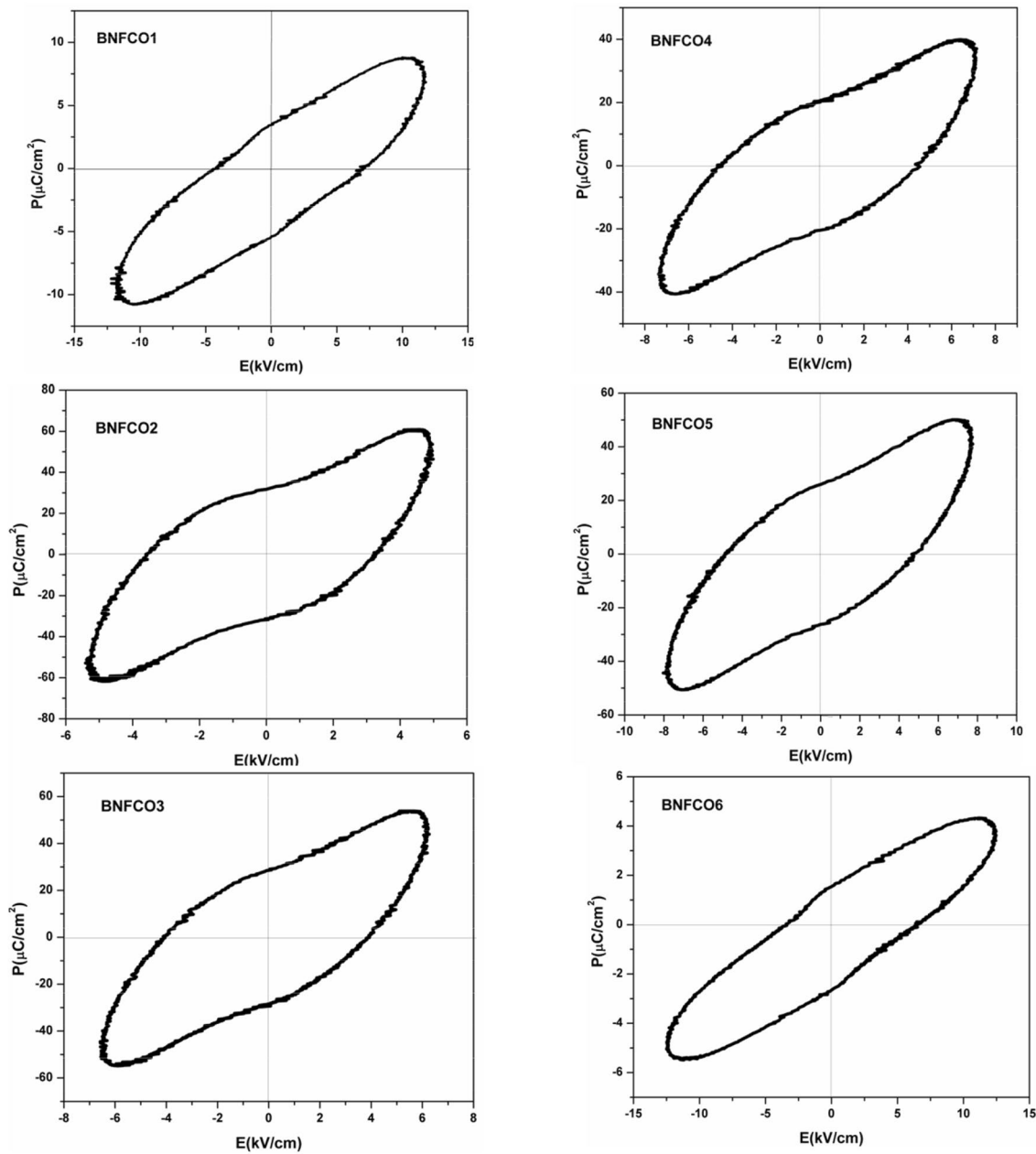
Fig. 5 Room temperature ferroelectric loops of BNFCO1, BNFCO2, BNFCO3, BNFCO4, BNFCO5 and BNFCO6

Table 2 Ferromagnetic and ferroelectric parameters of BFO, BNFCO1, BNFCO2, BNFCO3, BNFCO4, BNFCO5 and BNFCO6

Sample	H_c (G)	M_s (emu/g)	M_r (emu/g)	P_r (μC/ cm^2)	P_{max} (μC/ cm^2)
BNFCO1	371.73	0.263	0.0242	4.42	9.83
BNFCO2	474.56	0.38	0.052	20.96	61.49
BNFCO3	536.26	0.647	0.0882	28.52	53.24
BNFCO4	383.41	0.978	0.1165	17.38	40.12
BNFCO5	412.97	1.123	0.159	19.28	50.54
BNFCO6	1133.3	0.871	0.276	2.10	4.94

for the disruption of magnetism in BFO. With increase in the Nd doping concentration, we can observe the gradual enhancement in the magnetic parameters as seen from Table 2. Even for a low concentration 1% of Nd and 2% of Co, typical well saturated hysteresis loop appears. Since Nd is a rare earth magnet, the doping of Nd gradullay improves the magnetic structure of doped BFO. Moreover, the doping of Co, which is another magnetic atom, at Fe site further helps to improve the magnetic moment through Fe and Co ions. Moreover, (Nd, Co) doping changes the Fe–O bond and Fe–O–Fe bond angle (Table 1), which breaks
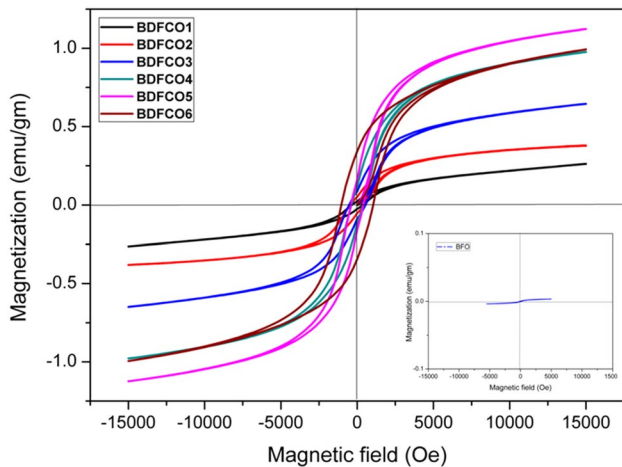
Fig. 6 Room temperature M-H curves of BNFCO1, BNFCO2, BNFCO3, BNFCO4, BNFCO5 and BNFCO6. The *inset* shows the M-H curve of BFO

the spin cycloid structure resulting in the enhanced magnetic behaviour. Also the double exchange interactions of Fe–O–Fe contribute to the improved magnetic characterisation of the doped samples. For higher Nd doping concentration such as 4 and 5%, striking enhancement is observed and for 6% abrupt hike in the magnetic parameters such as retentivity M_r and coercivity H_c are maximum compared to 4 and 5% is seen. The high coercivity of 6% is the evidence that internal strain has been induced in the BFO lattice due to high concentration of Nd doping and hence the high magnetic parameters of this doping are attributed to the strain induced magnetism. The strain caused by the distortion of high doping of Nd is also vividly explained from the Raman spectrum. So, the substitution Nd at Bi site and Co at Fe site results in a significant improvement in the magnetic properties of BFO. The remarkable development of the hysteresis loop with gradual Nd increase at Bi site reveals the striking influence of Nd and Co doping.

3 Conclusion

The Nd doping at Bi site with the concentration of 1–6% and Co 2% at Fe site were systematically investigated by preparing these samples by sol–gel method. The rhombohedral structure of all the samples were confirmed through XRD pattern and Raman spectrum. The XPS studies revealed the composition and purity of the samples. The XPS studies showed the low concentration of oxygen vacancies in the doped samples. The ratio of Fe^{3+} and Fe^{2+} proved that Fe^{3+} dominates over Fe^{2+}. The ferroelectric loops illustrate a remarkable improvement with Nd doping increase and this effect is due to the low concentration of

oxygen vacancies in the doped samples and also as result of reduction in the Fe–O–Fe hopping since concentration of Fe^{2+} is much less than Fe^{3+}. The magnetic M-H curve is well saturated for all the doped samples and with increase in Nd, the magnetic parameters are enhanced. In the case of 6%, the ferroelectric property is diminished which may due to the internal strain induced in the BFO lattice affecting the Bi–O vibration for high Nd level and also due to the large crystallite size. However, the magnetic parameters for 6% Nd doping are not affected as the magnetism could have been strain induced. In summary, the present investigation, provides a systematic analysis of the multiferroic properties of the Nd, Co codoped BFO in which the Nd is added in tiny amount in the Bi site with Co at Fe site. The development of the properties due to this type of doping and hence the possible tuning of the multiferroic properties have been revealed.

References

1. T. Kimura, T. Goto, H. Shintani, K. Ishizaka, T. Arima, Y. Tokura, Nature London **426**, 55 (2003)
2. N. Hur, S. Park, P.A. Sharma, J.S. Ahn, S. Guha, S.W. Cheong, Nature London **429**, 392 (2004)
3. N.A. Spaldin, M. Feibig, Science **309**, 391 (2005)
4. W. Erenstein, N.D. Mathur, J.F. Scott, Nature London **442**, 759 (2006)
5. M. Feibig, T. Lottermoser, D. Frohlich, A.V. Goltsev, R.V. Pisarev, Nature London **419**, 818 (2002)
6. F. Kubel, H. Schmid, Acta Crystallogr. Sect. B **B46**, 698 (1990)
7. P. Fischer, M. Polomska, I. Sosnowska, M. Szymanski, J. Phys. C **13**, 1931 (1980)
8. M. Feibeg, V.V. Palov, R.V. Pisarev, J. Opt. Soc. Am. B **22**, 96 (2005)
9. C. Quan, Y. Ma, Y. Han, X. Tang, M. Lu, W. Mao, J. Zhang, J. Yang, X. Li, W. Huang, J. Alloys Compd. **635**, 272 (2015)
10. N. Hernandez, V.A. Gonzalez-Gonzalez, I.B. Dzul-Bautista, J. Guitierrez, J.M. Barandiaran, I. Ruiz de Larramendi, R.F. Cienfyegos-Pelaes, U. Ortis-Mendez, J. Alloys Compd. **638**, 282 (2015)
11. C.M. Raghavan, J.W. Kim, S.S. Kim, T.K. Song, Appl. Phys. A **119**, 667 (2015)
12. C. M. Raghavan, J.W. Kim, S.S. Kim, Ceram. Int. **39**, 3563 (2013)
13. V.A. Khomchenko, L.C.J. Pereira, J.A. Paixao, J. Appl. Phys. **115**, 034102 (2014)
14. N. Hernandez, V.A. Gonzalez-Gonzalez, I.B. Dzul-Bautista, R.F. Cienfyegos-Pelaes, J.M. Barandiaran, J. Guitierrez, T. Hernandez, U. Ortis-Mendez, A.F. Garcia-Loera, J. Magn. Magn. Mater. **377**, 466 (2015)
15. S. Godara, N. Sinha, B. Kumar, Ceram. Int. **42**, 1782 (2016)
16. W. Mao, X. Wang, Y. Han, X. Li, Y. Li, Y. Wang, Y. Ma, X. Feng, T. Yang, J. Yang, W. Huang, J. Alloys Compd. **584**, 520 (2014)

17. K. Chakrabarti, K. Das, B. Sarkar, S. Ghosh, S.K. De, G. Sinha, J. Lahtinen, Appl. Phys. Lett. **101**, 042401 (2012)
18. R. Haumount, T. Kreisel, P. Bouvier, F. Hippert, Phys. Rev. B **73**, 132101 (2006)
19. J. Wu, J. Wang, Acta Mater. **58**, 1688 (2010)
20. P. Hermet, M. Goffinet, J. Kreisel, P. Ghosez, Phys. Rev. B **75**, 220102 (2007)
21. G.L. Yuan, S.W. Or, H.L.W. Chan, J. Appl. Phys. **101**, 064101 (2007)
22. M. Romero, R.W. Gomez, V. Marquina, J.L. Perez-Mazariego, R. Escamilla, Phys. Rev. B **443**, 90 (2014)
23. M. Aronniemi, J. Sainio, J. Lahtinen, Surf. Sci. **578**, 108 (2005)